This article has been accepted for inclusion in a future issue of this journal. Content is final as presented, with the exception of pagination.

Improved Inverted Organic Solar Cells With a Sol–Gel Derived Indium-Doped Zinc Oxide Buffer Layer

Aung Ko Ko Kyaw, *Student Member, IEEE*, Xiaowei Sun, *Senior Member, IEEE*, De Wei Zhao, *Student Member, IEEE*, Swee Tiam Tan, Yoga Divayana, and Hilmi Volkan Demir

***Abstract*—We studied sol–gel derived indium-doped zinc oxide (IZO) with various indium contents as a functional buffer layer in inverted polymer:fullerene bulk-heterojunction solar cell. The short-circuit current density was observed to increase by doping indium in pure ZnO buffer layer. The maximum current density was obtained with a 1 at.% indium doping. Although the open-circuit voltage and fill factor reduced slightly, the inverted organic solar cell with 1 at.% IZO buffer layer showed a power conversion efficiency of 3.3%, which is higher compared to that (2.94%) of the device with undoped ZnO buffer layer under illumination of AM1.5G. The better performance is due to combined effects of improvement in charge collection and higher optical transmittance of electrode/buffer layer stack.**

***Index Terms*—Indium-doped zinc oxide (IZO), inverted organic solar cell, sol–gel.**

I. Introduction

ORGANIC solar cells (OSCs) based on bulk-heterojunction (BHJ) concept are considered to be a promising candidate for the next generation solar cells because of light weight, mechanical flexibility, compatibility with roll-to-roll manufacturing, and potentially low cost. In a conventional structure of an OSC, indium tin oxide (ITO) modified with p-type poly (3,4-ethylene dioxythiophene):(polystyrene sulfonic acid) (PEDOT:PSS) is used as anode. The polarity of ITO can, however, be reversed by modifying with an n-type functional buffer layer, and only electrons are then exclusively collected by ITO electrode. Such device architecture, normally known as an inverted structure, has distinct advantages over the conventional one. The device stability is improved as a result of the elimination of acidic PEDOT:PSS, which destroys ITO [1], and the replacement of low-work-function metal with high-work-function metal top electrode, which prevents diffusion of air and moisture into organic active layer [2]. However, additional resistance resulted from the collection of charges via functional buffer layer leads to high series resistance in the device and reduction in short-circuit current density. Hence, further improvement of inverted architecture can be expected by reducing the resistivity of the functional buffer layer and optimizing the energy alignment between acceptor/buffer layer interfaces [3].

Indium-doped zinc oxide (IZO), which has previously been applied as a channel layer in thin-film transistor [4] and an interlayer for forming ohmic contact in UV LED [5], is a suitable candidate to be used as an n-type functional buffer layer to overcome the limitation of inverted OSC due to the fact that its resistivity is lower and transmittance is higher compared to undoped ZnO [6]. Such IZO further offers several benefits, and IZO can be deposited by low-cost solution-processing methods such as spray pyrolysis [7] and sol–gel techniques [8], which are compatible with solution-based processing of BHJ solar cells. The amount of dopant is also tunable by controlling the amount of precursors within a reasonable accuracy. However, only ZnO [9], TiO_2 [10], TiO_x [11], and Cs_2O_3 [12] have been used as n-type buffer layers in inverted OSCs to date. Different from previous works in the literature, in this paper, we employed IZO as an n-type buffer layer of inverted OSCs and manipulated the doping concentration to optimize the device performance. We demonstrated that the performance of inverted OSC is enhanced, especially in the short-circuit current density (J_{sc}), by replacing conventional ZnO with appropriately doped IZO buffer layer.

Manuscript received October 30, 2009; revised November 23, 2009 and December 14, 2009. This work was supported in part by the Ministry of Education, Singapore under Academic Research Fund under Grant RGM 44/06.

A. K. K. Kyaw, X. W. Sun, D. W. Zhao, and Y. Divayana are with the School of Electrical and Electronic Engineering, Nanyang Technological University, Singapore 639798, Singapore (e-mail: aung0069@ntu.edu.sg; exwsun@ntu.edu.sg; zhao0075@ntu.edu.sg; dyoga@ntu.edu.sg).

H. V. Demir is with the School of Electrical and Electronic Engineering and the School of Physical and Mathematical Sciences, Nanyang Technological University, Singapore 639798, Singapore (e-mail: hvdemir@ntu.edu.sg).

S. T. Tan is with the Institute of Microelectronics, Agency for Science, Technology and Research, Singapore 117685, Singapore (e-mail: tanst@ime.a-star.edu.sg).

Color versions of one or more of the figures in this paper are available online at http://ieeexplore.ieee.org.

Digital Object Identifier 10.1109/JSTQE.2009.2039200

II. Experimental Details

A. Sol–Gel Preparation

We first prepared IZO sol using zinc acetate dihydrate [$Zn(CH_3COO).2H_2O$] (99.95% Fluka) as precursor, indium chloride [$InCl_3$] (98% Aldrich) as dopant source, ethanol [CH_3CH_2OH] (99.5+% Aldrich) as solvent, and ethanolamine [$NH_2CH_2CH_2OH$] (99+% Sigma-Aldrich) as sol stabilizer [13]. Indium chloride contents used in the sol are 0, 1, 2, and 3 at.% of the precursor and the concentration of the sol was kept constant at 0.1 M. Zinc acetate dehydrate and indium chloride were first dissolved in ethanol and rigorously stirred for 2–3 h at 80 °C. Subsequently, ethanolamine was added to the solution followed by thorough mixing process with magnetic stirred for 12–15 h at 60 °C.

1077-260X/$26.00 © 2010 IEEE

Authorized licensed use limited to: ULAKBIM UASL - Bilkent University. Downloaded on June 03,2010 at 07:27:23 UTC from IEEE Xplore. Restrictions apply.

This article has been accepted for inclusion in a future issue of this journal. Content is final as presented, with the exception of pagination.

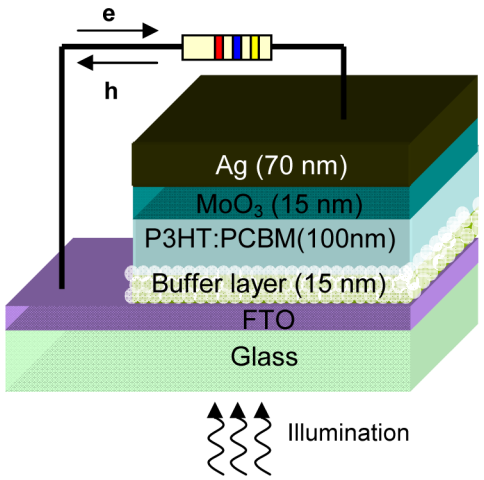

Fig. 1. Device structure of the inverted OSC illustrating the flow of charge. Numerical values inside the parentheses represent the thicknesses of corresponding layers.

B. Device Fabrication

The device architecture we studied is fluorine-doped SnO_2 (FTO)/buffer layer/polymer:fullerene blend/MoO_3/Ag as shown in Fig. 1. In our device architecture, we use FTO as bottom electrode instead of ITO, which is used in conventional OSC. Since the work function of FTO (4.4 eV) is higher than that of top electrode Ag (4.5 eV), internal electric field due to unsymmetrical electrode is promoting the flow of charge carriers. However, the work function of ITO (4.8–5.1 eV) is lower than that of Ag and the internal electric filed is opposing the flow of charge carriers. Therefore, for ITO bottom electrode, very high-work-function electrode such as Au is more suitable to be used as top electrode in inverted structure, yet Au is much more expensive than Ag. Therefore, we opt to use FTO and Ag as electrodes for our device. In our typical device fabrication process, a functional buffer layer was spin coated onto a precleaned FTO glass with a sheet resistance of 15 Ω/square from the sols in a low humidity environment (RH 13%). The coating step was repeated a few times to obtain desired thickness. As-deposited thin films were annealed at 350 °C for 1 h in air and colloidal thin films with a thickness of ∼15 nm were obtained. Then, the samples were transferred into a glove box and the active layer with a thickness of ∼100 nm was fabricated by spin coating the blend solution, made of poly (3-hexylthiophene)(P3HT) (Rieke Metals, Inc.) and 6,6-phenyl C_{61} butyric acid methyl ester (PCBM) (Nano-C) with a weight ratio of 1:1 in chlorobenzene (40 mg/ml), onto the buffer layer previously deposited. Finally, a 15-nm MoO_3 and a 70-nm Ag were deposited under 3×10^{-4} Pa by thermal evaporation through a shadow mask. The fabricated devices were post-annealed at 150 °C under N_2 ambient for 10 min.

C. Characterization and Simulation

Photovoltaic measurement was conducted by illuminating the devices under a solar simulator (Solar Light Company, Inc.) with an AM1.5G filter. The simulated light intensity was adjusted to 100 mW/cm^2 calibrated with a Thorlabs optical power meter. The current–voltage (*J–V*) characteristics were examined using a Keithley 2400 Sourcemeter. X-ray photoelectron spectroscopy (XPS) measurements were performed with a Kratos ESCA (model AXIS Ultra) using a monochromated Al K_α ($h\upsilon = 1486.7$ eV) X-ray source operated at 15 kV and 10 mA under 8.6×10^{-9} torr. XPS data were collected after etching for 10 min with Ar+ to eliminate the contamination on the surface. Tapping mode atomic force microscopic (AFM) images of IZO films and active layers were taken with Nanoscope IIIa (Digital Instruments) scanning probe microscope. The sheet resistance of IZO-modified FTO film was extracted by Hall effect measurement (BIO-RAD) with Van der Pauw geometry at room temperature. Al (80 nm) deposited by e-beam evaporation was used as contacts for Hall effect measurement. The optical transmittance and absorption spectra of the films were measured by UV-vis-NIR spectrophotometer system (PerkinElmer Lambda 950) with an integrating sphere to capture directly transmitted light and forward scattered light. External quantum efficiency (EQE) spectrum was measured using a Xenon light source with 300 mm focal length monochromator (Bentham). Optical electric field simulation was carried out by matrix methods proposed by Pettersson *et. al.*, using complex refractive index and thickness of individual layers as input parameters [14].

III. Results and Discussion

We verified the incorporation of indium compound in the IZO film with XPS prior to the device fabrication. The stoichiometry of the IZO films calculated from XPS spectra reveals that the actual indium content in IZO films derived from 1, 2, and 3 at.% $InCl_3$ precursor are 0.91%, 1.89%, and 3.2% respectively. Hence, it is worth mentioning that the actual dopant amount incorporated in the film can be controlled from the dopant source precursor within 10% accuracy. The surface morphologies of IZO films coated on FTO glass investigated by AFM are shown in Fig. 2. A significant change in morphology due to incorporation of IZO was not observed. The rms roughnesses of the films are 3.996, 2.537, 2.858, and 4.39 nm for IZO film with 0, 1, 2, and 3 at.% indium respectively. All IZO films with different indium contents show similar grain size.

Fig. 3 (a) and (b) shows the *J-V* curves of the resulting devices with different buffer layers and the extracted device parameters under illumination and in the dark, respectively. The variation in device performance is not significant in terms of open-circuit voltage (V_{oc}) and fill factor (FF). However, J_{sc} changes significantly due to buffer layer doping. J_{sc} of devices with IZO buffer layers containing 0, 1, 2, and 3 at.% indium contents are 8.392, 9.935, 9.307, and 8.924 mA/cm^2, respectively. The maximum J_{sc} is achieved at 1 at.% indium content.

The photocurrent generation process in OSC involves five major steps:

1) light absorption and exciton generation;
2) exciton diffusion to acceptor–donor interface;
3) exciton dissociation at acceptor–donor interface;
4) free-charge carriers transport to electrodes; and
5) charge collection at electrodes.

Authorized licensed use limited to: ULAKBIM UASL - Bilkent University. Downloaded on June 03,2010 at 07:27:23 UTC from IEEE Xplore. Restrictions apply.

This article has been accepted for inclusion in a future issue of this journal. Content is final as presented, with the exception of pagination.

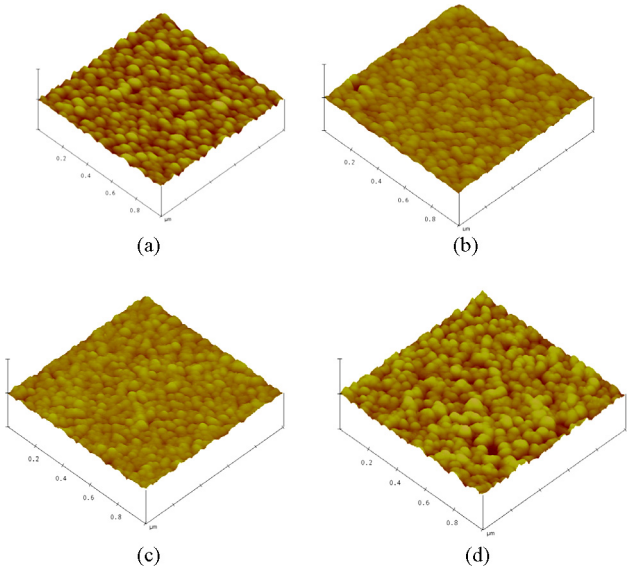

Fig. 2. AFM 3-D topographic images of buffer layers with (a) 0 at.%, (b) 1 at.%, (c) 2 at.%, and (d) 3 at.% indium content. Scan size was 1 μm $\times$ 1 μm.

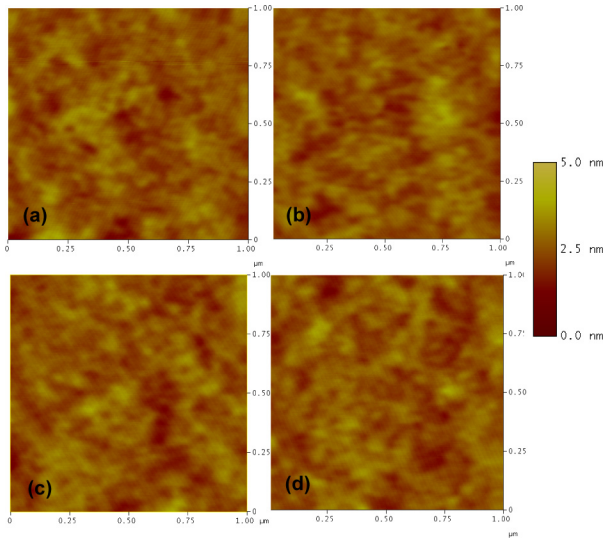

Fig. 4. AFM images of active layers fabricated on buffer layer with (a) 0 at.%, (b) 1 at.%, (c) 2 at.%, and (d) 3 at.% indium content. Scan size was 1 μm $\times$ 1 μm.

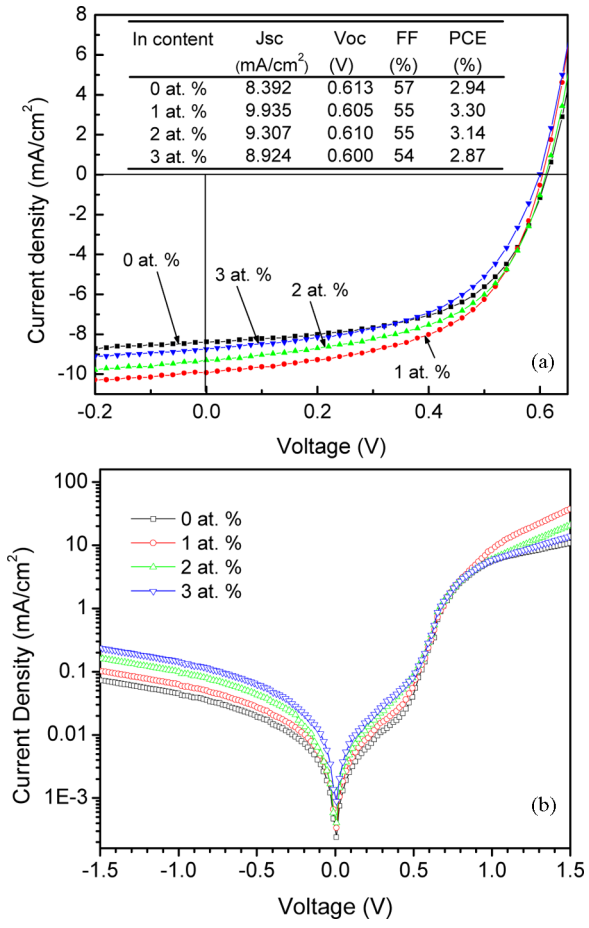

Fig. 3. *J–V* characteristics of devices, employing IZO films doped with various indium contents as the buffer layers (a) under simulated solar irradiation of AM 1.5 G (100 mW/cm^2) and (b) in the dark.

We can assume that exciton diffusion, exciton dissociation, and charge carriers transport are the same for all devices, supposing that the morphology and phase separation of BHJ is the same for all devices since we used the same acceptor and donor in the same solvent for all devices. This hypothesis can be verified with two experimental evidences. First, the morphology and roughness of the active layers fabricated on different buffer layers revealed by AFM measurement (see Fig. 4) are almost identical. The roughness (rms) values of the active layers on buffer layers with 0, 1, 2, and 3 at.% indium content are 0.381, 0.37, 0.37, and 0.394 nm, respectively. Second, the slope of dark *J–V* curve in intermediate positive voltage region (between 0.5 and 0.75 V) is the same, suggesting that internal bulk morphology (phase separation of donor/acceptor) is similar for all the devices [15]. Although the active layers were fabricated on different buffer layers, we observed that the thickness of all active layers was approximately controlled at 100 nm. In addition, the difference between the maximum and minimum roughness of buffer layers is only 1.85 nm, which is extremely small compared to the thickness of active layer. All these evidences imply that the variation of active layers in the fabricated devices is negligible and changes in J_{sc} are not due to active layer. Hence, the enhancement in J_{sc} can be attributed to charge collection at electrode and/or the improvement in optical transmittance of buffer layer that increases the net absorption of light in active layer.

As the free electrons at acceptor/buffer interface pass through the buffer layer before being collected at electrode, the conductivity of buffer layer is important for charge collection process. The average sheet resistance of 0, 1, 2, and 3 at.% indium containing IZO-coated FTO is 42.3, 35, 37.2, and 40.2 Ω/square respectively, suggesting that all IZO films are more favorable in transport of electron to FTO electrode than ZnO film and IZO with 1 at.% indium is the best among the buffer layers. It is worth mentioning that the trend in resistivity of the film is

Authorized licensed use limited to: ULAKBIM UASL - Bilkent University. Downloaded on June 03,2010 at 07:27:23 UTC from IEEE Xplore. Restrictions apply.

This article has been accepted for inclusion in a future issue of this journal. Content is final as presented, with the exception of pagination.

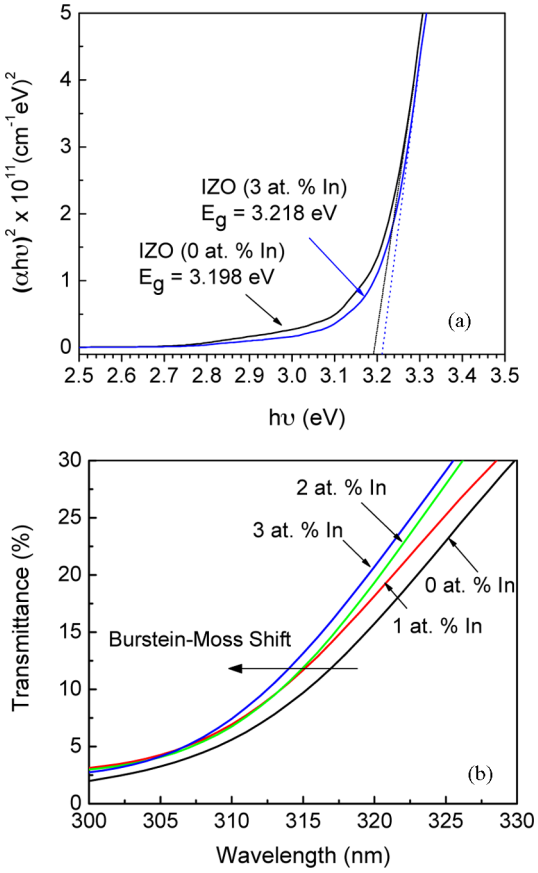

Fig. 5. (a) Plot of $(\alpha h\upsilon)^2$ against $h\upsilon$ for calculating band gap of the buffer layers. (b) Shift in transmittance of buffer layers near the absorption band edge due to increase in carrier concentration.

consistent with the previous reports on the dependency of IZO resistance on indium doping [13], [16]. The resistivity initially increases upon doping because dopant acts as additional charge carrier and increases the mobility, whereas it decreases again with the increase in dopant concentration due to the impurities (chlorine) from the precursor.

Another factor responsible for charge collection is the energy alignment at acceptor/buffer interface. The work function of buffer layer can be precisely measured with ultraviolet photoelectron spectroscopy (UPS) [17]. However, due to equipment availability, we calculated the optical band gap of various IZO films by extrapolating the straight line of $(\alpha h\upsilon)^2$ plot to $h\upsilon$-axis (where α and υ are the absorption coefficient and frequency of photon, respectively, which are extracted from absorption spectrum), as shown in Fig. 5(a) [18]. The observed band gap is increased from 3.198 to 3.218 eV with increasing indium concentration from 0 to 3 at.%. Moreover, theoretically, the Fermi level of an n-type semiconductor increases with carrier concentration [19]. The increase in carrier concentration of IZO films with increasing dopant can be clearly seen as the Burstein–Moss shift (blue shift) in the transmittance spectrum near absorption band edge, as shown in Fig. 5(b) [20]. Both facts suggest that the work function of buffer layer is decreased with increasing indium concentration. A decrease in work function of buffer layer reduces the energy barrier for electron to jump to the buffer

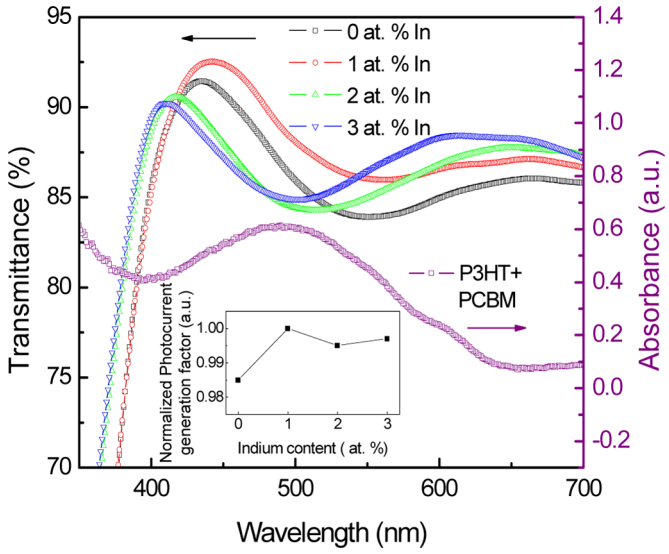

Fig. 6. Optical transmission spectra of IZO film with different indium contents (*Y*-axis—left) and absorption of P3HT:PCBM active layer (*Y*-axis—right) in the visible range. (Inset) The normalized photocurrent generation factor due to the changes in indium content of IZO buffer layer.

layer, favoring the charge collection process. Hence, IZO buffer layer is better than pure ZnO buffer layer for charge collection process.

As the light is incident from the FTO electrode, the optical transmittance of FTO/buffer layer stack alters the net absorption of photons in the active layer. A few experimental works have been proved that $J_{\rm sc}$ is increased due to the highly transparency of the under layer [21], [22]. The transmittance of combined glass substrate, FTO, and buffer layer in visible range and the absorbance of the active layer are shown in Fig. 6. It can be seen that the transmittance of IZO with 1 at.% indium is higher than that of undoped buffer layer. However, it is hard to compare between IZO with 0, 2, and 3 at.% indium because of mixed high and low transmittance in different regions of the spectrum. Therefore, we make use of the following equation to determine the effect of transmittance of buffer layer on $J_{\rm sc}$:

$$J_{\rm ph} = \int \frac{q\lambda}{hc}\eta_A(\lambda)\eta_{\rm int}S(\lambda)d\lambda \qquad (1)$$

where $J_{\rm ph}$, q, h, c, η_A, $\eta_{\rm int}$, and S represent photocurrent density, the elementary charge, Planck's constant, the speed of light, absorption efficiency, internal quantum efficiency, and spectrum of light from sun (simulator), respectively. Since q, h, c, and S are constants, the term $\int \lambda\eta_A(\lambda)d\lambda$, defined as photocurrent generation factor, causes the variation in $J_{\rm sc}$ besides $\eta_{\rm int}$. In order to take into account the effect of transmittance of buffer layer, we calculated η_A as the product of the absorbance of active layer and total transmittance (including substrate, FTO, and buffer layer), with a spectral integration range from 350 to 700 nm. The normalized photocurrent generation factor is shown in Fig 6 (inset). Since the optical interference due to the reflection of light from the counter electrode is important for thin films with thickness comparable to the wavelength of incident light, we also simulated the optical field

Authorized licensed use limited to: ULAKBIM UASL - Bilkent University. Downloaded on June 03,2010 at 07:27:23 UTC from IEEE Xplore. Restrictions apply.

This article has been accepted for inclusion in a future issue of this journal. Content is final as presented, with the exception of pagination.

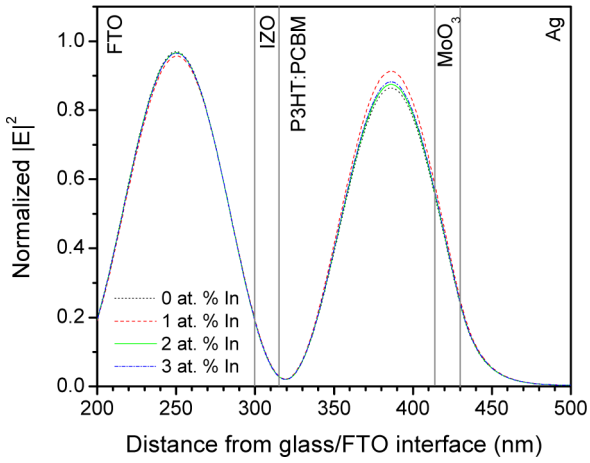

Fig. 7. Simulated optical field distribution inside the devices with buffer layers containing various indium contents for single-wavelength illumination at 535 nm. These devices have structure of glass (2.2 mm)/FTO (300 nm)/IZO (15 nm)/ P3HT:PCBM (100 nm)/MoO_3 (15 nm)/Ag (70 nm).

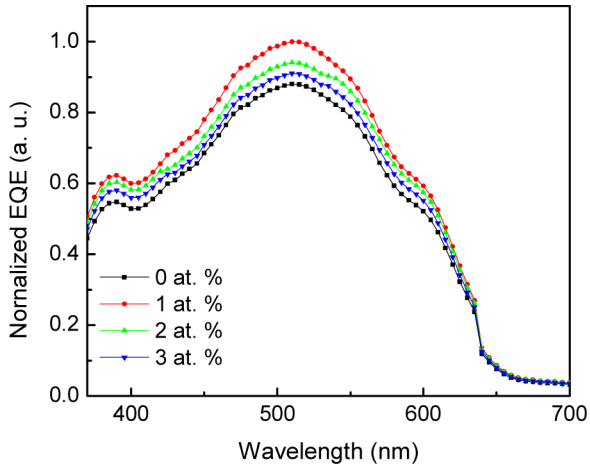

Fig. 8. Normalized EQE spectra of fabricated devices with different buffer layers containing various indium contents.

distribution inside the device for single-wavelength illumination at wavelength 535 nm. Although there is no shift in peak of optical intensity (modulus squared of the electric filed $|E|^2$), the maximum intensity $|E|^2$ in the active layer is observed in device with 1 at.% indium containing buffer layer (see Fig. 7). The variation in optical electric field distribution inside the active layer follows the trend in transmittance of electrode/buffer layer stack at 535 nm. From both transmittance of electrode/buffer layer stack and optical distribution simulation, it can be seen that J_{sc} is also affected by the optical property of buffer layer although the contribution is not very significant.

The combined factors of charge collection (transport in buffer layer and energy alignment) and light absorption (due to transmittance of buffer layer) contribute to J_{sc} of inverted OSCs in the experiment. Since IZO with 1 at.% indium is advantageous for all these factors, the device fabricated with this buffer layer shows the highest J_{sc} among the devices. Although IZO with 3 at.% indium is the most beneficial to the electron transfer from acceptor to buffer layer due to better energy alignment, J_{sc} of that device is lower than former due to the drawback in resistivity (carrier transport in buffer layer), and probably due to rough buffer layer that causes nonuniform electric field inside the buffer layer and disturbs current flow in device operation [23]. In Fig. 8, the trend of overall EQE spectra agrees well with that of J_{sc}. The variation in J_{sc} also correlates well with the change in series resistances (R_s) of devices, which are 9.85, 6.71, 8.95, and 9.5 $\Omega\cdot cm^2$ for the devices employing buffer layers with 0, 1, 2, and 3 at.% indium content, respectively. The changes in R_s due to doping buffer layer can also be clearly seen in the dark *J–V* curves at high applied voltage region, where the shape of *J–V* curve is mainly dominated by R_s [see Fig. 3(b)]. The device with lowest R_s shows the highest dark current at high voltage region and vice versa.

We observed slight deterioration in FF due to indium incorporation although variation is trivial. A few groups reported that smooth buffer layer increases the FF of OSCs [22], [24]. However, in the case of devices fabricated from IZO with 1 and 2 at.% indium, the FF is decreased despite a similar roughness. Therefore, some other reason must be responsible for low FF. Since R_s of devices with IZO buffer layer is lower than that of device with ZnO layer, a slight decline in FF is caused by decrease in shunt resistance (R_{sh}), which can be attributed to electron injection barrier. Since the buffer layer serves as electron collection in photocurrent generation process as well as electron injection under forward bias, a decrease in work function due to indium dopant not only increases the charge collection for solar cell, but also facilitates the electron injection into diode under forward bias. The raise in electron injection capability increases the diode (leakage) current under forward bias, which is opposed to photocurrent direction. The leakage current due to electron injection barrier lowering can be observed in the dark *J–V* curves at negative and low positive voltage region [see Fig. 3(b)]. Hence, in the case of devices fabricated from IZO with 1 and 2 at.% indium, we attribute low FF to the leakage current that reflects as low R_{sh} in the *J–V* curve. For the device fabricated from IZO with 3 at.% indium, even lower FF can be ascribed to both leakage current and high roughness.

Although the work function of buffer layer is decreased, we observe that V_{oc} is not increased. According to the literature [25], the large concentration of electrons at the cathode due to low electron injection barrier decreases V_{oc}. Hence, we suppose that the former effect compensates the latter one and V_{oc} is relatively stable in all devices. Despite slight degradation in V_{oc} and FF, due to significant increase in J_{sc}, overall power conversion efficiency (PCE) of devices fabricated from IZO with 1 and 2 at.% indium is higher than that of device with ZnO buffer layer. However, in the case of device fabricated from IZO with 3 at.% indium, slight increase in J_{sc} is offset by low FF and overall PCE is lower than ZnO-based device.

It is worth mentioning that MoO_3 thickness of 15 nm yielded very low efficiency in our previous study [26], yet gives much higher efficiency in this study. We attribute this to different combinations of materials and thicknesses of layers employed in two studies, since the optical filed distribution is much dependent on the optical property and thickness of individual

Authorized licensed use limited to: ULAKBIM UASL - Bilkent University. Downloaded on June 03,2010 at 07:27:23 UTC from IEEE Xplore. Restrictions apply.

This article has been accepted for inclusion in a future issue of this journal. Content is final as presented, with the exception of pagination.

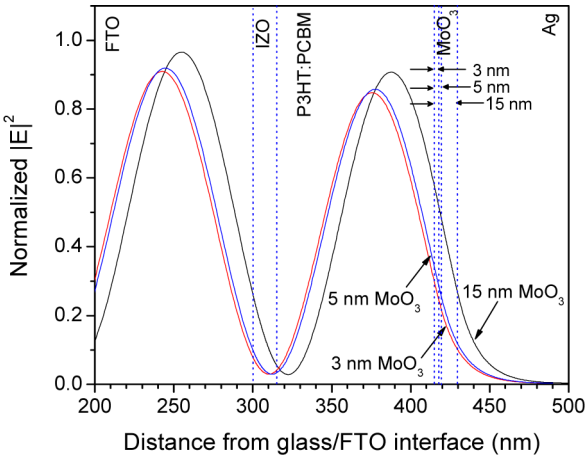

Fig. 9. Simulated optical filed distribution inside the individual layers of device for illumination at 520 nm. The device structure used in the simulation is glass (2.2 mm)/FTO (300 nm)/IZO (1 at.% In)(15 nm)/ P3HT:PCBM (100 nm)/MoO_3 (x nm)/Ag (70 nm) with $x = 3$, 5, and 15 nm.

layers. In this study [glass (2.2 mm)/FTO (300 nm)/IZO (15 nm)/ P3HT:PCBM (100 nm)/MoO_3/Ag (70 nm)], the simulation result shows that MoO_3 thickness of 15 nm yields higher intensity peak than MoO_3 thickness of 3 or 5 nm despite a shift to Ag electrode (see Fig. 9). On the other hand, in the previous study [glass (1.1 mm)/ITO (130 nm)/Ca (1 nm)/P3HT:PCBM (85 nm)/MoO_3/Ag (100 nm)], MoO_3 thickness of 15 nm rendered not only lower intensity of peak, but also shifted the peak to electrode, resulting to very low efficiency.

IV. Conclusion

In summary, J_{sc} of inverted OSC is influenced by the n-type buffer layer due to the combined factors contributed from charge collection and light harvesting. A decrease in work function of buffer layer resulting from the increase in dopant is beneficial to the charge collection, yet has slight negative impact on V_{oc} and FF due to election injection barrier lowering. This kind of trend agrees well with previous findings in conventional OCSs in which J_{sc} is increased, but V_{oc} and FF (or only V_{oc}) are declined due to high-conductivity p-type buffer layer [23], [25]. On the basis of previous findings and our observations, it can be concluded that, regardless of conventional or inverted OSCs, a buffer layer controls the tradeoff between J_{sc} and V_{oc} and FF, which can be compromised by manipulating doping level, in other word, the energy level and conductivity of the buffer layer. The doping level of the buffer layer must be well optimized to achieve the optimum power conversion efficiency of OSC.

Acknowledgment

The authors would like to thank L. D. Sun for the X-ray photoelectron spectroscopy measurement and P. Liu for optical simulation.

References

[1] M. P. d. Jong, L. J. van I. doorn, and M. J. A. de Voigt, "Stability of the interface between indium-tin-oxide and poly(3,4-ethylenedioxythiophene)/poly(styrenesulfonate) in polymer light-emitting diodes," *Appl. Phys. Lett.*, vol. 77, pp. 2255–2257, 2000.

[2] F. C. Krebs and K. Norman, "Analysis of the failure mechanism for a stable organic photovoltaic during 10000 h of testing," *Prog. Photovoltaics*, vol. 15, pp. 697–712, 2007.

[3] L. M. Chen, Z. Hong, G. Li, and Y. Yang, "Recent progress in polymer solar cells: Manipulation of polymer:fullerene morphology and the formation of efficient inverted polymer solar cells," *Adv. Mater.*, vol. 21, pp. 1434–1449, 2009.

[4] B. Yaglioglu, H. Y. Yeom, R. Beresford, and D. C. Paine, "High-mobility amorphous In_2O_3 – 10 wt% ZnO thin film transistors," *Appl. Phys. Lett.*, vol. 89, pp. 062103-1–062103-3, 2006.

[5] K. Y. Ban, H. G. Hong, D. Y. Noh, T. Y. Seong, J. O. Song, and D. Kim, "Use of an indium zinc oxide interlayer for forming Ag-based Ohmic contacts to p-type GaN for UV-light-emitting diodes," *Semicond. Sci. Technol.*, vol. 20, pp. 921–924, 2005.

[6] P. M. R. Kumar, C. S. Kartha, K. P. Vijayakumar, T. Abe, Y. Kashiwaba, F. Singh, and D. K. Avasthi, "On the properties of indium doped ZnO thin films," *Semicond. Sci. Technol.*, vol. 20, pp. 120–126, 2005.

[7] J. Wienke and A. S. Booij, "ZnO:In deposition by spray pyrolysis—Influence of the growth conditions on the electrical and optical properties," *Thin Solid Films*, vol. 516, pp. 4508–4512, 2008.

[8] E. J. L. Arredondo, A. Maldonado, R. Asomoza, D. R. Acosta, M. A. M. Lira, and M. de la L. Olvera, "Indium-doped ZnO thin films deposited by the sol-gel technique," *Thin Solid Films*, vol. 490, pp. 132–136, 2005.

[9] M. S. White, D. C. Olson, S. E. Shaheen, N. Kopidakis, and D. S. Ginley, "Inverted bulk-heterojunction organic photovoltaic device using a solution-derived ZnO underlayer," *Appl. Phys. Lett.*, vol. 89, pp. 143517-1–143517-3, 2006.

[10] G. K. Mor, K. Shankar, M. Paulose, O. K. Varghese, and C. A. Grimes, "High efficiency double heterojunction polymer photovoltaic cells using highly ordered TiO_2 nanotube arrays," *Appl. Phys. Lett.*, vol. 91, pp. 152111-1–152111-3, 2007.

[11] C. Waldauf, M. Morana, P. Denk, P. Schilinsky, K. Coakley, S. A. Choulis, and C. J. Brabec, "Highly efficient inverted organic photovoltaics using solution based titanium oxide as electron selective contact," *Appl. Phys. Lett.*, vol. 89, pp. 233517-1–233517-3, 2006.

[12] G. Li, C.-W. Chu, V. Shrotriya, J. Huang, and Y. Yang, "Efficient inverted polymer solar cells," *Appl. Phys. Lett.*, vol. 88, pp. 253503-1–253503-3, 2006.

[13] J. H. Lee and B. O. Park, "Transparent conducting ZnO:Al, In and Sn thin films deposited by the sol-gel method," *Thin Solid Films*, vol. 426, pp. 94–99, 2003.

[14] L. A. A. Pettersson, L. S. Roman, and O. Inganas, "Modeling photocurrent action spectra of photovoltaic devices based on organic thin films," *J. Appl. Phys.*, vol. 86, pp. 487–496, 1999.

[15] C. Waldauf, M. C. Scharber, P. Schilinsky, J. A. Hauch, and C. J. Brabec, "Physics of organic bulk heterojunction devices for photovoltaic applications," *J. Appl. Phys.*, vol. 99, pp. 104503-1–104503-6, 2006.

[16] M. Ohyama, H. Kozuka, and T. Yoko, "Sol-gel preparation of transparent and conductive aluminum-doped zinc oxide films with highly preferential crystal orientation," *J. Amer. Ceram. Soc.*, vol. 81, pp. 1622–1632, 1998.

[17] H.-H. Liao, L.-M. Chen, Z. Xu, G. Li, and Y. Yang, "Highly efficient inverted polymer solar cell by low temperature annealing of Cs_2CO_3 interlayer," *Appl. Phys. Lett.*, vol. 92, pp. 173303-1–173303-3, 2008.

[18] S. T. Tan, B. J. Chen, X. W. Sun, X. Hu, X. H. Zhang, and S. J. Chua, "Properties of polycrystalline ZnO thin films by metal organic chemical vapor deposition," *J. Cryst. Growth*, vol. 281, pp. 571–576, 2005.

[19] S. M. Sze and K. K. Ng, *Physics of Semiconductor Devices*. Hoboken, NJ: Wiley, 2007, ch. 1.

[20] H. Hiramatsu, W. S. Seo, and K. Koumoto, "Electrical and optical properties of radio-frequency-sputtered thin films of (ZnO)InO," *Chem. Mater.*, vol. 10, pp. 3033–3039, 1998.

[21] A. K. K. Kyaw, X. W. Sun, C. Y. Jiang, G. Q. Lo, D. W. Zhao, and D. L. Kwong, "An inverted organic solar cell employing a sol-gel derived ZnO electron selective layer and thermal evaporated MoO_3 hole selective layer," *Appl. Phys. Lett.*, vol. 93, pp. 221107-1–221107-3, 2008.

[22] Y. Zhou, F. Zhang, K. Tvingstedt, S. Barrau, F. Li, W. Tian, and O. Inganas, "Investigation on polymer anode design for flexible polymer solar cells," *Appl. Phys. Lett.*, vol. 92, pp. 233308-1–233308-3, 2008.

[23] S. W. Tong, C. F. Zhang, C. Y. Jiang, G. Liu, Q. D. Ling, E. T. Kang, D. S. H. Chan, and C. Zhu, "Improvement in the hole collection of polymer solar cells by utilizing gold nanoparticle buffer layer," *Chem. Phys. Lett.*, vol. 453, pp. 73–76, 2008.

Authorized licensed use limited to: ULAKBIM UASL - Bilkent University. Downloaded on June 03,2010 at 07:27:23 UTC from IEEE Xplore. Restrictions apply.

This article has been accepted for inclusion in a future issue of this journal. Content is final as presented, with the exception of pagination.

[24] R. Steim, S. A. Choulis, P. Schilinsky, and C. J. Brabec, "Interface modification for highly efficient organic photovoltaics," *Appl. Phys. Lett.*, vol. 92, pp. 093303-1–093303-3, 2008.
[25] F. L. Zhang, A. Gadisa, O. Inganas, M. Svensson, and M. R. Andersson, "Influence of buffer layers on the performance of polymer solar cells," *Appl. Phys. Lett.*, vol. 84, pp. 3906–3908, 2004.
[26] D. W. Zhao, P. Liu, X. W. Sun, S. T. Tan, L. Ke, and A. K. K. Kyaw, "An inverted organic solar cell with an ultrathin Ca electron-transporting layer and MoO_3 hole-transporting layer," *Appl. Phys. Lett.*, vol. 95, pp. 153304-1–153304-3, 2009.

Aung Ko Ko Kyaw (S'09) received the B.Eng. degree (First Class Honors) in electrical and electronic engineering in 2007 from Nanyang Technological University, Singapore, where he is currently working toward the Ph.D. degree at the School of Electrical and Electronic Engineering.

From 2007 to 2008, he was a Research Officer with the Institute of Microelectronics, Agency for Science, Technology and Research, Singapore. His current research interests include ZnO nanostructure and organic photovoltaics.

Mr. Kyaw is a Student Member of the Society for Information Display Singapore and Malaysia Chapter.

Xiaowei Sun (SM'99) was born in Beijing, China. He received the B.Eng., M.Eng., and Ph.D. degrees in photonics from Tianjin University, Tianjin, China, and the second Ph.D. degree in electrical and electronic engineering from The Hong Kong University of Science and Technology, Kowloon, Hong Kong.

From 1986 to 1994, he was with Tianjin University. From 1994 to 1998, he was with The Hong Kong University of Science and Technology. Since 1998, he has been with the Division of Microelectronics, School of Electrical and Electronic Engineering, Nanyang Technological University, Singapore, as an Assistant Professor, where he was promoted to Associate Professor in 2006. His research interests include metal–organic chemical vapor deposition growth of ZnO, display technologies, and nanotechnology.

Dr. Sun is a Member of the Society for Information Display (SID). He is the Founding Chair of SID Singapore and Malaysia Chapter.

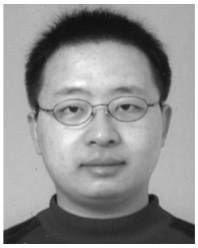

De Wei Zhao (S'09) received the M.S. degree in optical engineering from Beijing Jiaotong University, Beijing, China, in 2007. He is currently working toward the Ph.D. degree in the School of Electrical and Electronic Engineering, Nanyang Technological University, Singapore.

He was engaged in the research on organic LEDs with multiple layers and their mechanisms. His current research interests include organic solar cells with tandem and inverted structures, as well as the organic/inorganic hybrid solar cells such as carbon nanotubes.

Mr. Zhao is a Student Member of the Society for Information Display Singapore and Malaysia Chapter and the IEEE Photonics Society Singapore Chapter.

Swee Tiam Tan was born in Perak, Malaysia, in 1980. He received the B.Eng. and Ph.D. degrees from Nanyang Technological University, Singapore, in 2003 and 2007, respectively.

He was involved in ZnO thin films and nanostructures grown by metal–organic chemical vapor deposition. Since 2007, he has been a Senior Research Engineer with the Semiconductor Process Technologies Laboratory, Institute of Microelectronics, Agency for Science, Technology and Research, Singapore. He has authored or coauthored more than 30 peer-reviewed journal publications. His current research interest includes growth, characterization, and application of semiconducting oxide films and nanostructures.

Yoga Divayana received the B.Eng. and Ph.D. degrees from Nanyang Technological University, Singapore, in 2005 and 2008, respectively.

He is currently a Postdoctoral Researcher in the School of Electrical and Electronic Engineering, Nanyang Technological University. His research interests include fabrication of organic LED, exciton diffusion in organic material, and organic solar cell.

Dr. Divayana was the recipient of 2008 Singapore Millennium Foundation Fellowship Award and the 2008 IEEE Lasers and Electro-Optics Society Graduate Student Fellowship Award.

Hilmi Volkan Demir received the B.Sc. degree in electrical and electronics engineering from Bilkent University, Ankara, Turkey, in 1998, and the M.S. and Ph.D. degrees in electrical engineering from Stanford University, Stanford, CA, in 2000 and 2004, respectively.

During September 2004, he was a faculty member in the Department of Electrical and Electronics Engineering and the Department of Physics, Bilkent University. Since August 2009, he has been an Associate Professor at the School of Electrical and Electronic Engineering (Microelectronics Division) and the School of Physical and Mathematical Sciences (Physics and Applied Physics Division), Nanyang Technological University, Singapore. His current research interests include the development and demonstration of high-quality solid-state lighting and high-efficiency photovoltaics using semiconductor quantum dot nanocrystals, resonance energy transfer-driven devices, plasmonic devices, biomimetic optoelectronic devices, and bioimplant metamaterial sensors.

Dr. Demir was a recipient of the 2009 National Research Foundation Fellowship Award and the 2007 European Young Investigator Award (European Science Foundation ESF-EURYI). He was also a recipient of the 2005 European Union Marie Curie Fellowship Award, the 2006 Distinguished Young Scientist Award of Turkish National Academy of Sciences (TUBA-GEBIP), the 2008 Parlar Foundation Young Scientist Award, and the 2009 Türkiye Bilimsel ve Teknolojik Araştırma Kurumu Young Scientist Award. He was a recipient of the 2007 JCI World First Prize in academic achievement and leadership as a young scientist for The Outstanding Young Persons Awards (TOYP Awards) of Junior Chamber International (JCI International Federation of Young Leaders and Entrepreneurs).

Authorized licensed use limited to: ULAKBIM UASL - Bilkent University. Downloaded on June 03,2010 at 07:27:23 UTC from IEEE Xplore. Restrictions apply.